2024 IEEE/RSJ International Conference on Intelligent Robots and Systems (IROS)
October 14-18, 2024. Abu Dhabi, UAE

Interpretation of Legged Locomotion in Underwater Robots based on Rimless Wheel Model

Yuetong He and Fumihiko Asano

Abstract— **Inspired by the fascinating underwater locomotion of cephalopods such as octopuses, this research explores the possibility of using legged robots in underwater environments. Using a rimless wheel model, we investigated their navigation and adaptation capabilities in a dynamic fluid environment. Through sophisticated numerical simulations, we reproduce legged robot behaviours such as walking underwater and jumping over uneven seabed terrain. Our research aims to provide valuable insights for the development of versatile underwater robotic systems suitable for various applications in ocean exploration and surveying.**

I. INTRODUCTION

Robotics research has long been inspired by the extraordinary dexterity and speed demonstrated by legged animals in terrestrial locomotion [1]–[3]. Although much of this research has traditionally focused on land-based applications, there is significant potential to extend the capabilities of legged robots to the marine environment, particularly in the area of underwater exploration [4]. In order to meet the growing demand for energy and raw materials, and out of concern for the conservation and sustainable use of the Earth's finite resources, more and more companies are turning their attention from land to the depths of the oceans in search of new resources and exploitation potential. The need for robots capable of exploring and operating in extreme deep-sea environments without causing damage to marine ecosystems is increasing the demand for innovative underwater robotics [5]. Conventional underwater robots, known for their efficient propulsion mechanisms and streamlined design, are able to swim nimbly in deep water and are suitable for deep-sea exploration and monitoring missions [6]. Their main limitations, however, lie in their complexity of control and limited payload. Walking robots, on the other hand, have unique advantages when dealing with complex terrain, such as rocks on the seabed or shipwrecks [7] [8]. They are able to walk stably on irregular surfaces and perform precise operations such as sampling or cleaning. These advantages of walking robots make them ideal for performing precise tasks in underwater operations, especially in areas that traditional underwater robots cannot reach or maneuver effectively. These characteristics allow walking robots to play an important role in areas such as underwater archaeology, biological sampling or seabed infrastructure maintenance.

The authors are with the Graduate School of Advanced Science and Technology, Japan Advanced Institute of Science and Technology, 1-1 Asahidai, Nomi, Ishikawa 923-1292, Japan {s2220012,fasano}@jaist.ac.jp

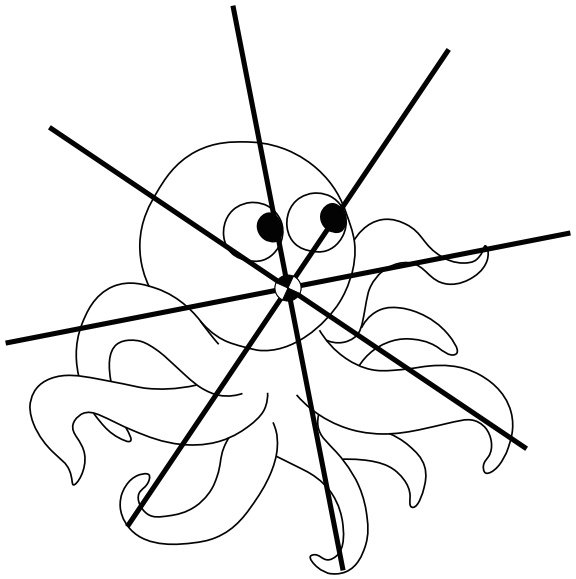

Fig. 1. Conceptual diagram of octopus-Inspired rimless wheel locomotion

Cephalopods, such as octopuses and squids, have several ways of moving, one of which is jet propulsion [9] [10]. It is fast, flexible and efficient. Many current underwater robots use this type of propulsion [11]–[14]. Despite these advantages, it also has some disadvantages, including high energy consumption, environmental disturbances, complex structure and influence from the external environment. Arm swimming is also a mode of locomotion for octopuses. It allows the octopus to freely adjust its speed and direction and is excellent for fine manoeuvring or positioning [15]–[17]. In spite of these advantages, arm swimming can be slower than other swimming modes and can consume more energy when swimming continuously for long periods of time. In addition, we found that the octopus employs lifting six tentacles in moving across the seafloor and using two tentacles for bipedal walking instead of swimming [18]. Compared to swimming, walking allows the octopus to manoeuvre more nimbly between rocks, seaweed and other obstacles on the seafloor, helping to avoid collisions and injuries. In addition, when an octopus encounters uneven terrain on the seabed, it will choose to jump to get over the uneven area. This jumping behaviour allows the octopus to quickly traverse the depression and avoid getting stuck in potholes or traps, demonstrating the flexibility and adaptability of seafloor walking in the face of complex seafloor terrain.

Although studies have investigated the hydrodynamic con-

979-8-3503-7769-9/24/$31.00 ©2024 IEEE

tribution of simulated underwater octopus arm movements [19] [20], research into their effects in underwater environments, particularly on underwater walking, is still limited. Recent advances in extending the Spring-Loaded Inverted Pendulum (SLIP) model to aquatic environments offer an approach to address this gap. Max P. Austin extended the SLIP model to accommodate motion on land, underwater and on the water surface by incorporating fluid dynamics [21]. T. G. Thuruthel used the SLIP model to explore energy stopping and starting on complex terrains [22]. M. Calisti applied the SLIP model in legged robots, focusing on mimicking the dynamics of jumping and running [23]. These developments lay a foundation for this study, which combines the SLIP model with hydrodynamics to explore the dynamics of underwater walking for rimless wheel robot.

First, Chapter 2 introduces a model of an 8-legged rimless wheel robot and explores basic motion to understand its behavior. Second, Chapter 3 uses numerical simulations to model the robot's underwater walking on a slope, analyzing how the liquid environment affects its passive walking. We also simulate two cephalopod movement modes—bipedal walking and jumping—on different seabed terrains by adjusting control parameters. By analyzing these modes, we explore the robot's potential in complex underwater environments and provide insights for designing more adaptable underwater robots. The research objective is to establish a generalized walking-in-liquid model for robots in underwater surveying, ocean exploration, and related fields.

II. MATHEMATICAL MODEL

This chapter commences with an exposition of an underwater walking robot comprising a rimless wheel and a flywheel. The subsequent sections present its equations of motion and elucidate its control methodology. Finally, a comparative analysis is conducted between the two modes of motion exhibited by the robot, along with an examination of its performance under diverse operating conditions.

A. Model Assumptions

Fig. 2 illustrates the structure and parameters of the underwater walking robot, which will be elaborated on in the subsequent discussion.

- (x,z) serves as the coordinates of the centre of mass of the rimless wheel.
- θ_1 defines the angular position of the stance-leg with respect to the vertical.
- θ_2 defines the angular position of the fly wheel with respect to the vertical.
- L denotes the distance from the tip of the leg frame to the centre of the rimless wheel.
- α describes the relative angle between adjacent leg frames. In this rimless wheel comprised of 8 leg frames, so that $\alpha = \pi/4$ [rad].
- m_1 and I_1 represent the mass and moment of inertia of the rimless wheel, respectively.
- m_2 and I_2 represent the mass and moment of inertia of the fly wheel, respectively.

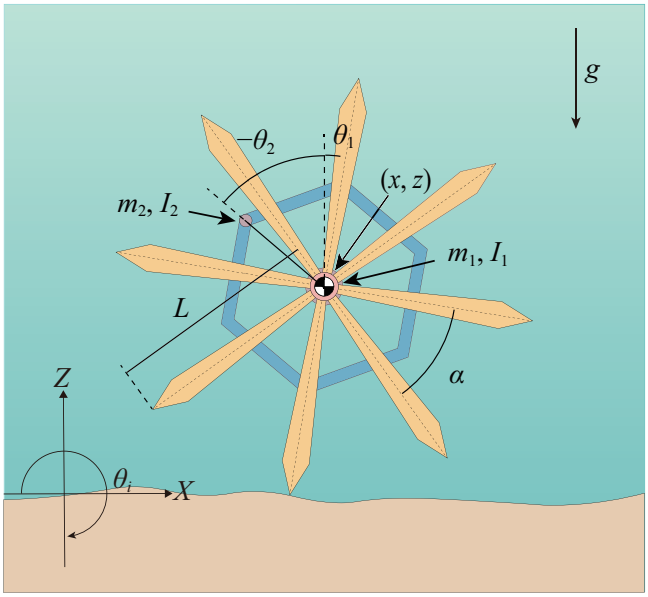

Fig. 2. Mathematical model of robot on the surface of water

B. Equation of Motion

Let $\boldsymbol{q} = \begin{bmatrix} x & z & \theta_1 & \theta_2 \end{bmatrix}^{\mathrm{T}}$ be the generalized coordinate vector, the robot equation of motion then becomes

$$\boldsymbol{M}\ddot{\boldsymbol{q}} + \boldsymbol{h} = \boldsymbol{J}_c^{\mathrm{T}}\boldsymbol{\lambda} + \boldsymbol{F} + \boldsymbol{S}u, \tag{1}$$

$$\boldsymbol{J}_c\dot{\boldsymbol{q}} = \boldsymbol{0}. \tag{2}$$

Here, $\boldsymbol{M}$ represents the inertia matrix, $\boldsymbol{h}$ represents the combination of centrifugal force, Coriolis force and gravity terms, as:

$$\boldsymbol{M} = \begin{bmatrix} m_1 & 0 & 0 & 0 \\ 0 & m_1 & 0 & 0 \\ 0 & 0 & I_1 & 0 \\ 0 & 0 & 0 & I_2 \end{bmatrix}, \quad \boldsymbol{h} = \begin{bmatrix} 0 \\ m_1 g \\ 0 \\ 0 \end{bmatrix}. \tag{3}$$

The first term on the right side of Eq. (1), $\boldsymbol{J}_c^{\mathrm{T}}\boldsymbol{\lambda}$ signifies the constraint condition term, where

$$\boldsymbol{J}_c = \begin{bmatrix} 1 & 0 & L\cos\theta_1 & 0 \\ 0 & 1 & -L\sin\theta_1 & 0 \end{bmatrix}. \tag{4}$$

The second term to the right side of Eq. (1), F represents the force of the water in the system, the details are shown below.

The third term on the right side of Eq. (1) represents the control input vector defined as:

$$\boldsymbol{S} = \begin{bmatrix} 0 & 0 & 1 & -1 \end{bmatrix}^{\mathrm{T}}. \tag{5}$$

Here, $\boldsymbol{S}$ represents the driving matrix and $\boldsymbol{u}$ denotes the control input between θ_1 and θ_2. Combining Eq. (1) and Eq. (2) , we can deduce the floor reaction force, as:

$$\boldsymbol{\lambda} = -\boldsymbol{X}_c^{-1}\boldsymbol{J}_c\boldsymbol{M}^{-1}(\boldsymbol{F} + \boldsymbol{S}u - \boldsymbol{h}) + \dot{\boldsymbol{J}}_c\dot{\boldsymbol{q}}, \tag{6}$$

where $\boldsymbol{X}_c = \boldsymbol{J}_c\boldsymbol{M}^{-1}\boldsymbol{J}_c^{\mathrm{T}}$. Incorporating Eq. (6) representing the floor reaction force into Equation of Motion Eq.(1) yields:

$$\boldsymbol{M}\ddot{\boldsymbol{q}} = \boldsymbol{Y}_c(\boldsymbol{S}u + \boldsymbol{F} - \boldsymbol{h}) + \boldsymbol{J}_c^{\mathrm{T}}\dot{\boldsymbol{J}}_c\dot{\boldsymbol{q}}, \tag{7}$$

where $\boldsymbol{Y}_c = \boldsymbol{I}_4 - \boldsymbol{J}_c^{\mathrm{T}} \boldsymbol{X}_c^{-1} \boldsymbol{J}_c \boldsymbol{M}^{-1}$.

C. Equation of Collision

Since we are using an inelastic collision model and have excluded the case of a two-legged support. After the support leg leaves the ground, the swing leg will collide with the ground, at which point the following equations will be satisfied:

$$\boldsymbol{M}\dot{\boldsymbol{q}}^{+} = \boldsymbol{M}\dot{\boldsymbol{q}}^{-} + \boldsymbol{J}_I^{\mathrm{T}}\lambda_I, \tag{8}$$

$$\boldsymbol{J}_I\dot{\boldsymbol{q}}^{+} = \boldsymbol{0}_{2\times 1}. \tag{9}$$

where

$$\boldsymbol{J}_I = \begin{bmatrix} 1 & 0 & L\cos(\theta_1 - (i-1)\alpha & 0 \\ 0 & 1 & -L\sin(\theta_1 - (i-1)\alpha & 0 \end{bmatrix}, \tag{10}$$

here, $i \in (1,2,3\cdots 8)$ represents the index of the robot leg, with the support leg designated as 1 and numbered counterclockwise.

By establish a correlation between Eq. (8) and Eq. (9), resulting in the derivation of the Lagrange multiplier vector λ_I, as

$$\boldsymbol{\lambda}_I = -\boldsymbol{X}_I^{-1}\boldsymbol{J}_I\dot{\boldsymbol{q}}^{-}, \tag{11}$$

where $\boldsymbol{X}_I = \boldsymbol{J}_I\boldsymbol{M}^{-1}\boldsymbol{J}_I^{\mathrm{T}}$.

By substituting Eq. (11) into Eq. (8), we derive the updated velocity vector $\dot{\boldsymbol{q}}^{+}$ following the collision, yielding:

$$\dot{\boldsymbol{q}}^{+} = (\boldsymbol{I}_4 - \boldsymbol{M}^{-1}\boldsymbol{J}_I^{\mathrm{T}}\boldsymbol{X}_I^{-1}\boldsymbol{J}_I)\dot{\boldsymbol{q}}^{-}. \tag{12}$$

In the context of our exploration into a gait pattern where the robot encounters potential buoyancy-induced jumps during water traversal, it becomes crucial to ensure that upon transitioning from the support leg to the swing leg, after changing leg, the new support leg coordinate vector $\boldsymbol{q}^{+}$ becomes:

$$\boldsymbol{q}^{+} = \begin{bmatrix} x^{-} \\ z^{-} \\ \theta_1^{-} - (i-1)\alpha \\ \theta_2^{-} \end{bmatrix}. \tag{13}$$

D. Forces with water

To facilitate the analysis of the robot's motion in a water environment, we make the simplifying assumption that the water remains completely static without generating any waves or flows.

When operating in water, the robot experiences two primary forces: buoyancy, denoted as:

$$F_b = \rho g V, \tag{14}$$

and resistance generated by the water during its motion, represented by :

$$\boldsymbol{F}_d = \frac{1}{2} C_d \rho \dot{\boldsymbol{q}}^2 \boldsymbol{A}. \tag{15}$$

Here, ρ is the mass density of water, $\boldsymbol{v}$ is the flow velocity relative to the robot, V is the volume of the robot, A is constant which represent the cross sectional area of the robot in water, and C_d is a dimensionless coefficient of the drag.

$$\boldsymbol{F} = \boldsymbol{J}_b^T \boldsymbol{F}_b + \boldsymbol{F}_d, \tag{16}$$

Here, $\boldsymbol{J}_b = \begin{bmatrix} 0 & 1 & 0 & 0 \end{bmatrix}$. To simplify the model, we do not consider the effect of additional mass and lift on the system.

E. Control Method

To delve into the fundamental characteristics of the model and minimize the influence of control parameters, we opt for a straightforward approach by implementing a forward velocity control for the robot, the control output can be expressed as follows: $\theta_1 = \boldsymbol{C}\boldsymbol{q} = \begin{bmatrix} 0 & 0 & 1 & 0 \end{bmatrix}\boldsymbol{q}$.

The second-order derivative with respect to time is then given by:

$$\ddot{\theta}_1 = \boldsymbol{C}\ddot{\boldsymbol{q}} = \boldsymbol{C}\boldsymbol{M}^{-1}(\boldsymbol{S}\boldsymbol{u} + \boldsymbol{F} - \boldsymbol{h}). \tag{17}$$

Here, K_{D} and K_{P} are the derivative and proportional gains. To achieve stable and uniform forward motion of the robot, we devised a straightforward track for the rimless wheel, outlined as follows:

$$\theta_{1\mathrm{d}}(t) = \dot{\theta}_{1\mathrm{d}}t, \quad \ddot{\theta}_{1\mathrm{d}}(t) = 0. \tag{18}$$

Similarly, the control input for tracking $\theta_1(t)$ to $\theta_{1\mathrm{d}}(t)$ is obtained using:

$$N = \ddot{\theta}_{1\mathrm{d}} + K_{\mathrm{D}}(\dot{\theta}_{1\mathrm{d}} - \dot{\theta}_1) + K_{\mathrm{P}}(\theta_{1\mathrm{d}} - \theta_1). \tag{19}$$

F. Designed target trajectory

In order to make the foot move smoothly from $\boldsymbol{\theta}_{1s}$ at $t = 0$ to $\boldsymbol{\theta}_{1e}$ at $t = T$, the following fifth-order function of time is used:

$$\boldsymbol{\theta}_{1\mathrm{d}}(t) = \sum_{k=0}^{5} a_k t^k. \tag{20}$$

The boundary conditions from $t = 0$ to $t = T$ are as follows:

$$\begin{aligned} &\boldsymbol{\theta}_{1\mathrm{d}}(0) = \boldsymbol{\theta}_{1\mathrm{s}}, \quad \dot{\boldsymbol{\theta}}_{1\mathrm{d}}(0) = \dot{\boldsymbol{\theta}}_1^{-}, \quad \ddot{\boldsymbol{\theta}}_{1\mathrm{d}}(0) = 0, \\ &\boldsymbol{\theta}_{1\mathrm{d}}(T) = \boldsymbol{\theta}_{1\mathrm{e}}, \quad \dot{\boldsymbol{\theta}}_{1\mathrm{d}}(T) = n\alpha/T_{\mathrm{set}}, \quad \ddot{\boldsymbol{\theta}}_{1\mathrm{d}}(T) = 0. \end{aligned} \tag{21}$$

Each coefficient of Eq. (20) can be written as follows:

$$\begin{aligned} a_0 &= \boldsymbol{\theta}_{1\mathrm{s}}, \quad a_1 = \dot{\boldsymbol{\theta}}_1^{-}, \quad a_2 = 0, \\ a_3 &= \frac{-6\dot{\boldsymbol{\theta}}_1^{-}T_{\mathrm{set}} - 4\alpha - 10(\boldsymbol{\theta}_{1\mathrm{s}} - \boldsymbol{\theta}_{1\mathrm{e}})}{T_{\mathrm{set}}^3}, \\ a_4 &= \frac{8\dot{\boldsymbol{\theta}}_1^{-}T_{\mathrm{set}} + 7\alpha + 15(\boldsymbol{\theta}_{1\mathrm{s}} - \boldsymbol{\theta}_{1\mathrm{e}})}{T_{\mathrm{set}}^4}, \\ a_5 &= \frac{-3\dot{\boldsymbol{\theta}}_1^{-}T_{\mathrm{set}} + 2\alpha + 6(\boldsymbol{\theta}_{1\mathrm{s}} - \boldsymbol{\theta}_{1\mathrm{e}})}{T_{\mathrm{set}}^5}. \end{aligned} \tag{22}$$

Here, t represents the time parameter, which is reset to zero at each instance of stance-leg exchange, while T_{set} refers to the target step period, corresponding to the time required for the completion of the control cycle.

III. NUMERICAL SIMULATIONS

To explore the intricate dynamics of fluid drag in robotic locomotion, a numerical simulation was initiated. The initial parameter is set to $\boldsymbol{q} = \begin{bmatrix} 0 & 0.5 & -\pi & 0 \end{bmatrix}^{\mathrm{T}}$, the other parameters used are shown in Table I.

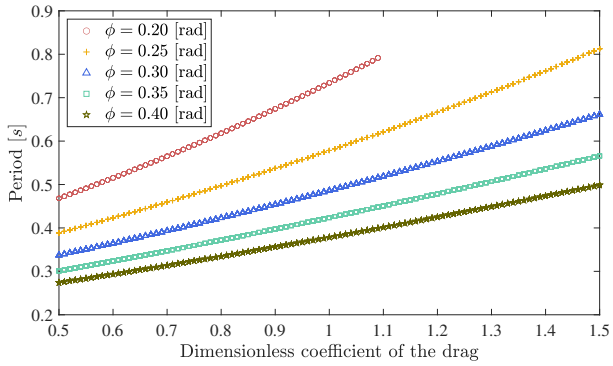

(a) Step period

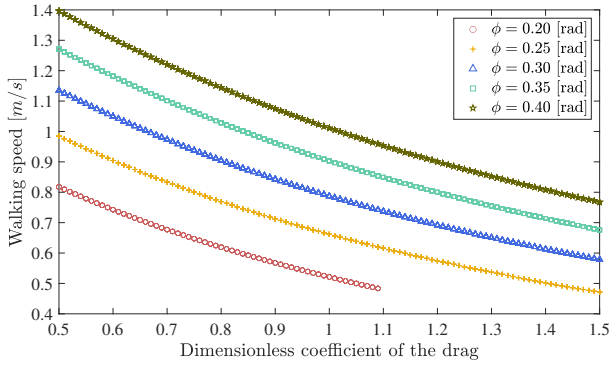

(b) Walking speed

Fig. 3. Simulation results of the walking gait corresponding to the increase of the dimensionless coefficient of drag C_d of the liquid

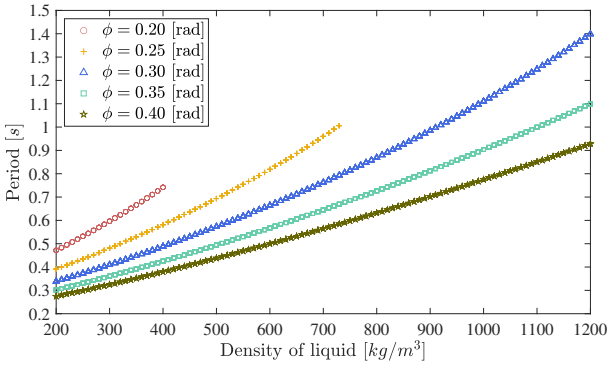

(a) Step period

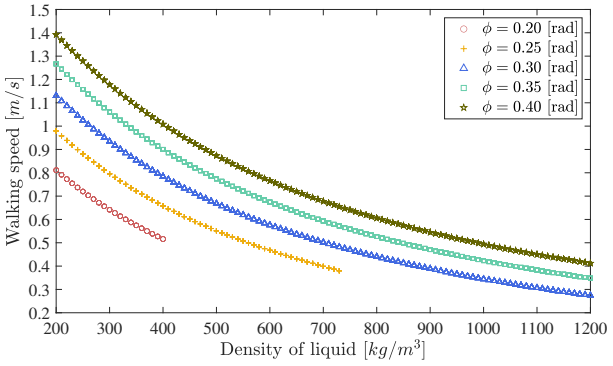

(b) Walking speed

Fig. 4. Simulation results of the walking gait corresponding to the increase of the density ρ of the liquid

A. *Simulation and improvement of water walking*

Fig. 3(a) and Fig. 3(b) show the nuanced effects of varying the dimensionless drag coefficients on both period and walking speed. The horizontal axis, delimitated as the dimensionless drag coefficient, spans the gamut from 0.5 to 1.5. It is worth noting that the dimensionless drag coefficient of water is typically around 1.5. These figures show five different data trajectories, each representing a different angle of ground inclination expressed as ϕ, ranging from 0.20 to 0.40. Each trajectory is annotated with different symbols and colours, making it easy to distinguish between the data. Obviously, as the drag coefficient increases, the speed of the passive walking robot slows down, accompanied by a noticeable lengthening of the gait cycle. This trend indicates that as the drag coefficient increases, the resistance within the fluid medium also increases, leading to a longer time required to complete a gait cycle. Furthermore, for identical drag coefficients, an increase in the angle of inclination leads to faster locomotion. This phenomenon can be attributed to the increase in the projection of the gravitational component onto the slope, providing the robotic system with a greater propulsive force to overcome the drag forces exerted by the fluid medium.

On the other hand, this graph in Fig. 4(a) and Fig. 4(b) show the relationship between the density of the liquid [kg/m³] and the robot's period and walking speed . The horizontal axis represents the density of the liquid ranging from 200 [kg/m³] to 1200 [kg/m³]. The walking speed decreases with increasing liquid density and drag coefficient, indicating a negative correlation. This may be due to the increased upward buoyancy force on the robot in higher density liquids.

A comparative analysis shows that density and drag coefficient have a similar effect on walking speed and period. As these two parameters increase, the walking speed decreases while the period increases and the walking efficiency of the robot is affected.

There are some breakpoints in the figure, such as when $\phi = 0.2$ [rad] , C_d is greater than 1.1 [N·s/m] or ρ is greater than 400 [kg/m³]. These missing parts represent cases of walking failure. This means that when the fluid resistance or density is too high, the robot is subjected to too much resistance in the x and z directions, resulting in the robot not being able to walk passively due to the component of gravity.

TABLE I

PHYSICAL PARAMETERS OF A SEX-LEGGED ROBOT

m_1	2.0	kg
L	0.25	m
C_d	1.5	N·s/m
ρ_{water}	1000.0	kg/m^3
T_{set}	0.7	s
K_{D}	40	s^{-1}
K_{P}	400	s^{-2}

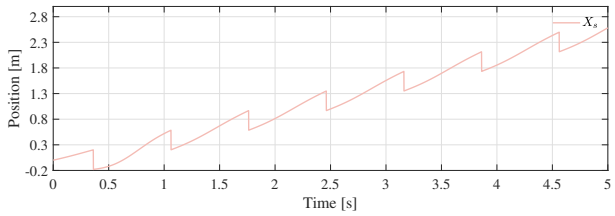

(a) The horizontal coordinates of the robot stance-leg x_s

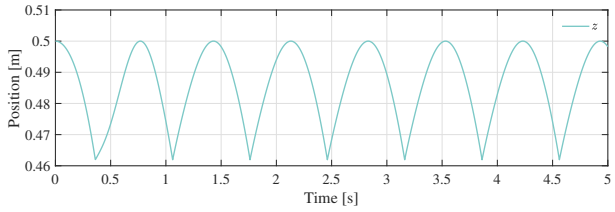

(b) Height of the centre of the robot z

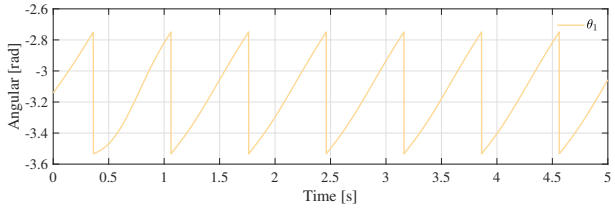

(c) The angle of the robot's feet with the vertical direction θ_1

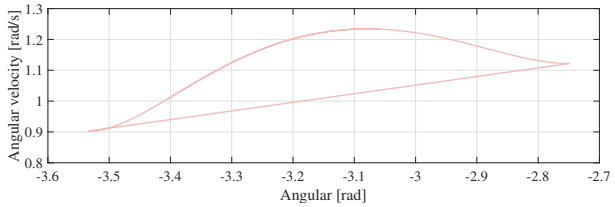

(d) Steady-state phase-plane plot

Fig. 5. Simulation results of rimless robot walking underwater

To address this issue, a control input will be implemented to enable the robot to follow the target trajectory outlined in Chapter II. By incorporating this control strategy, the robot will be able to actively walking through the environment, effectively overcoming the limitations imposed by excessive fluid drag or density.

B. Walking underwater by controlling the angle of stance-leg

Fig. 5(a) shows the variation over time of the transverse coordinates of the grounding point of the rimless wheel robot in the horizontal direction. The position of the robot's center of mass gradually increases from an initial position of -0.2 [m] to a final approximation of 2.8 [m] over the observation time of 5 [s]. The vertical axis represents the position in metres, which shows a gradual step-like curve. This gradual change is due to the fact that the robot's position is set to zero and then increased each time the stance-leg is grounded.

Fig. 5(b) shows the periodic variation of the centre of mass position over time in the vertical direction for the robot. The position of the center of mass varies between 0.46 [m] and 0.51 [m], showing regular periodic oscillations. This periodic variation may be related to the robot's walking rhythm, as well as the leg movement pattern.

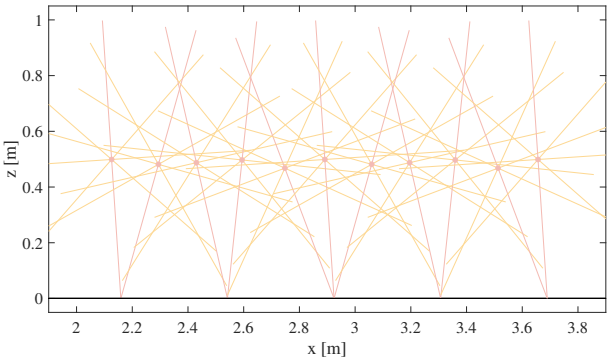

(a) Walking mode

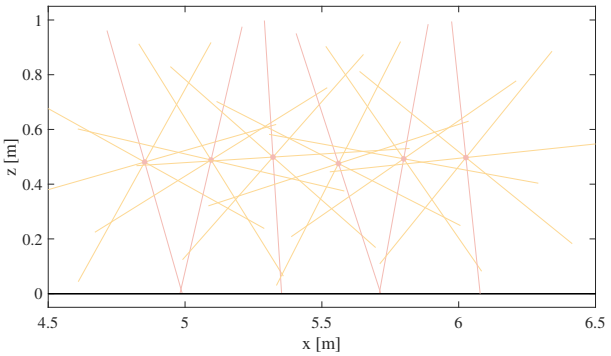

(b) Hopping mode

Fig. 6. Schematic diagram of the rimless wheel robot moving forward underwater

Fig. 5(c) shows how the angle of the stance-leg with respect to the vertical direction of the rimless wheel robot varies with time. The angle changes from -3.6 [rad] to -2.6 [rad]. The curves in the figure show that the change in angle is also periodic, mirroring the periodic change in the position of the center of mass in Fig. 5(b).

Fig. 5(d) shows the relationship between angle and angular velocity for the rimless wheel robot. The horizontal coordinates represent the angle in radians, ranging from -3.6 to -2.7 [rad]. The vertical coordinate represents the angular velocity in radians per second, ranging from 0.8 to 1.3 [rad/s]. The angle and angular velocity of the robot form a closed loop during a cycle, indicating that the robot's motion remains stable.

C. Walking mode and jumping mode

The SR (Specifc Resistance) is a dimensionless quantity used to evaluate the efficiency of walking. SR is calculated as follows:

$$SR = \frac{p}{mgv}, \tag{23}$$

where m is the total mass of the robot, v is the forward speed of the robot, and p is the average power, which is given by:

$$p = \frac{1}{T}\int_0^T \left| u\left(\dot{\theta}_1 - \dot{\theta}_2\right)\right| \mathrm{d}t, \tag{24}$$

where T is the total time of walking.

Fig. 6(a) shows the stick figure when the robot is rotated by an angle of α in one cycle. According to the previous

section, the robot is able to walk stably underwater in this scenario. When T_{set} is set to 0.5 [s], the SR of the robot reaches 0.78, indicating that its motion is relatively smooth in this scenario. Despite this, if the robot experiences a large angular change in a short period of time, such as a sudden change from a smooth walking state to a larger angle, the robot will rapidly accumulate a large angular velocity and generate a large force. The robot can be made to generate a jumping mode with both feet off the ground, as shown in Fig. 6(a). In jumping mode, the robot's trajectory changes significantly, and its velocity and motion are significantly different from those in smooth walking. As the water resistance is inversely proportional to the square of the speed, the speed of the robot increases in the jumping mode, which in turn leads to a significant increase in the resistance applied. In this case, the SR reaches a high value of 4.11, indicating a significant increase in the effort required by the robot in jumping mode.

IV. CONCLUSION AND FUTURE WORK

In this paper, we examine the motion behavior of a rimless wheel robot in a liquid medium and analyze the influences through numerical simulations. First, the horizontal and vertical trajectories of the robot in the passive walking state were examined, and it was found that they exhibited discernible periodic variations, which reflected the stability and periodicity of the robot's gait. The effects of liquid density and dimensionless drag coefficient on the robot's walking speed and period were further analyzed, and it was found that an increase in both density and drag coefficient resulted in a decrease in walking speed and an increase in period. Furthermore, we examined the robot's ability to transition between motion modes during large angular changes. Our findings revealed that the robot can transition from a steady walking state to a jumping mode with both feet off the ground, resulting in notable alterations to the trajectory and the drag force applied. In particular, we calculated the specific resistance and observed that the required inputs to the robot increase significantly in the jumping mode, potentially compromising the stability and efficiency of the robot.

As for future work, in order to address the efficiency and stability of the robot's walking in liquid media, we will further optimise the structural design of the robot to have a shape that is more adaptable to underwater walking. And we will optimise the control algorithm, for example by changing the shape of the robot and controlling the buoyancy force applied to the robot in real time, to improve its walking efficiency and stability adapted to different density and resistance conditions. Finally, real machine experiments will be carried out and applied in practical areas such as ocean exploration and underwater rescue to further verify its applicability in complex environments.

REFERENCES

[1] P. Biswal and P. K. Mohanty, "Development of quadruped walking robots: A review," *Ain Shams Engineering Journal*, vol. 12, no. 2, pp. 2017–2031, 2021.

[2] M. F. Silva and J. T. Machado, "A literature review on the optimization of legged robots," *Journal of Vibration and Control*, vol. 18, no. 12, pp. 1753–1767, 2012.

[3] C. D. Bellicoso, M. Bjelonic, L. Wellhausen, K. Holtmann, F. Günther, M. Tranzatto, P. Fankhauser, and M. Hutter, "Advances in real-world applications for legged robots," *Journal of Field Robotics*, vol. 35, no. 8, pp. 1311–1326, 2018.

[4] M. Dunbabin and L. Marques, "Robots for environmental monitoring: Significant advancements and applications," *IEEE Robotics Automation Magazine*, vol. 19, no. 1, pp. 24–39, 2012.

[5] G. Picardi, M. Chellapurath, S. Iacoponi, S. Stefanni, C. Laschi, and M. Calisti, "Bioinspired underwater legged robot for seabed exploration with low environmental disturbance," *Science Robotics*, vol. 5, no. 42, p. eaaz1012, 2020.

[6] R. Bogue, "Underwater robots: a review of technologies and applications," *Industrial Robot: An International Journal*, vol. 42, no. 3, pp. 186–191, 2015.

[7] G. Picardi, A. Astolfi, D. Chatzievangelou, J. Aguzzi, and M. Calisti, "Underwater legged robotics: Review and perspectives," *Bioinspiration & Biomimetics*, vol. 18, no. 3, p. 031001, 2023.

[8] L. Wang, Y. Lu, Y. Zhang, W. Chen, X. Zhao, and F. Gao, "Design and soft-landing control of underwater legged robot for active buffer landing on seabed," *Ocean Engineering*, vol. 266, p. 112764, 2022.

[9] R. M. Alexander, *Principles of animal locomotion*. Princeton university press, 2003.

[10] E. J. Anderson and M. A. Grosenbaugh, "Jet flow in steadily swimming adult squid," *Journal of Experimental Biology*, vol. 208, no. 6, pp. 1125–1146, 2005.

[11] C. Tang, W. Ma, B. Li, M. Jin, and H. Chen, "Cephalopod-inspired swimming robot using dielectric elastomer synthetic jet actuator," *Advanced Engineering Materials*, vol. 22, no. 4, p. 1901130, 2020.

[12] C. Christianson, Y. Cui, M. Ishida, X. Bi, Q. Zhu, G. Pawlak, and M. T. Tolley, "Cephalopod-inspired robot capable of cyclic jet propulsion through shape change," *Bioinspiration & biomimetics*, vol. 16, no. 1, p. 016014, 2020.

[13] J. M. Gosline and M. E. DeMont, "Jet-propelled swimming in squids," *Scientific American*, vol. 252, no. 1, pp. 96–103, 1985.

[14] F. G. Serchi, A. Arienti, and C. Laschi, "Biomimetic vortex propulsion: toward the new paradigm of soft unmanned underwater vehicles," *IEEE/ASME Transactions On Mechatronics*, vol. 18, no. 2, pp. 484–493, 2012.

[15] E. L. Kennedy, K. C. Buresch, P. Boinapally, and R. T. Hanlon, "Octopus arms exhibit exceptional flexibility," *Scientific reports*, vol. 10, no. 1, p. 20872, 2020.

[16] Y. Yekutieli, R. Mitelman, B. Hochner, and T. Flash, "Analyzing octopus movements using three-dimensional reconstruction," *Journal of neurophysiology*, vol. 98, no. 3, pp. 1775–1790, 2007.

[17] G. Levy, T. Flash, and B. Hochner, "Arm coordination in octopus crawling involves unique motor control strategies," *Current biology*, vol. 25, no. 9, pp. 1195–1200, 2015.

[18] C. L. Huffard, F. Boneka, and R. J. Full, "Underwater bipedal locomotion by octopuses in disguise," *Science*, vol. 307, no. 5717, pp. 1927–1927, 2005.

[19] M. Calisti, F. Corucci, A. Arienti, and C. Laschi, "Dynamics of underwater legged locomotion: modeling and experiments on an octopus-inspired robot," *Bioinspiration & biomimetics*, vol. 10, no. 4, p. 046012, 2015.

[20] M. Calisti, M. Giorelli, G. Levy, B. Mazzolai, B. Hochner, C. Laschi, and P. Dario, "An octopus-bioinspired solution to movement and manipulation for soft robots," *Bioinspiration & biomimetics*, vol. 6, no. 3, p. 036002, 2011.

[21] T. George Thuruthel, G. Picardi, F. Iida, C. Laschi, and M. Calisti, "Learning to stop: a unifying principle for legged locomotion in varying environments," *Royal Society Open Science*, vol. 8, no. 4, p. 210223, 2021.

[22] M. P. Austin and J. E. Clark, "The fluid field slip model: Terrestrial-aquatic dynamic legged locomotion," in *2021 IEEE International Conference on Robotics and Automation (ICRA)*. IEEE, 2021, pp. 4948–4954.

[23] M. Calisti and C. Laschi, "Morphological and control criteria for self-stable underwater hopping," *Bioinspiration & biomimetics*, vol. 13, no. 1, p. 016001, 2017.